NEXT-GENERATION INSAR GROUND-TRUTH DATA AND TECHNIQUES: INITIAL RESULTS

Sean M. Buckley[1], Paul Vincent[2], and Krishnavikas Gudipati[1]

University of Texas at Austin[1], Lawrence Livermore National Laboratory[2]

Sponsored by National Nuclear Security Administration
Office of Nonproliferation Research and Engineering
Office of Defense Nuclear Nonproliferation

Contract No. DE-FC52-03NA99566[1], W-7405-ENG-48[2]

ABSTRACT

The purpose of this study is to assess the capability of next-generation interferometric synthetic aperture radar (InSAR) satellite data and processing techniques to improve remotely-sensed ground truth associated with seismic source location, depth, and characterization. Initial project work has focused on the implementation of InSAR time series algorithms and their application to European Remote Sensing (ERS) synthetic aperture radar (SAR) data already in-hand. In an approach utilizing an ensemble of interferograms and singular value decomposition solution methods, a set of interferograms is used to construct a history of time-varying deformation, e.g., seasonal centimeter-scale subsidence variations superimposed on long-term constant subsidence rates. In addition, a coherent scatterer technique may be used to separate undesirable phase contributions from sub-centimeter deformation signatures on isolated coherent InSAR pixels. These time series approaches show promise in improving the signal-to-noise (SNR) ratio in data sets with atmospheric and decorrelation noise sources. The new Envisat satellite, with its increased number of operating modes as compared with ERS, is also providing SAR data over regions of interest to this study. These new processing approaches and data will be applied to several nuclear test sites as well as to moderate earthquakes used as calibration events; and their improvements documented.

OBJECTIVES

The goal of this study is to assess new satellite SAR data and InSAR processing techniques for improvements to current remotely-sensed ground truth (GT) collection capability for determining seismic source location, depth and characterization. Specifically, we are (a) applying InSAR time series analysis to sets of ERS and Envisat radar interferograms, (b) evaluating SAR data from several new acquisition modes offered by the European Envisat satellite, and (c) using InSAR results to constrain geophysical source modeling to improve determinations of seismic source location, depth, and mechanism.

RESEARCH ACCOMPLISHED

This paper presents results derived as part of initial development of two InSAR time series techniques: a linear inversion of a database of interferograms and InSAR processing of isolated coherent scatterers. Although results are shown for Phoenix, Arizona, our ongoing work involves the application of these techniques to several target seismic source regions throughout the world for which we possess ERS SAR data. In addition, we will make use of several new imaging modes available from the Envisat SAR satellite.

Linear Inversion of a Set of Interferograms

Recent InSAR research has focused on extracting time-variable deformation from a set of interferograms spanning overlapping periods of times. The result of these techniques is a history of deformation relative to a given reference image date, at each of the subsequent SAR acquisition dates, and broadly applied to areas of generally good coherence.

In developing a linear inversion solution based on least squares and singular value decomposition approach [Usai, 2001; Schmidt and Bürgmann, 2003], we invert 28 interferograms spanning 17 SAR acquisition dates (Figure 1, refer to Gudipati, Buckley and Wilson [2004] for additional details). The resulting 7-year time series (Figure 2 and Figure 3) reveals seasonal variations believed to be related to groundwater fluctuations. These subtle variations in deformation over time reveal important geophysical information not readily accessible through comparison of individual interferograms.

As part of ongoing work, 120 interferograms corresponding to 16 SAR acquisitions over the Nevada Test Site are being reduced for use in the time series and coherent scatterer InSAR assessment. A preliminary time series result shows cumulative displacement over the Nevada Test Site from June 11, 1995, to June 16, 1997, (Figure 4). The synthetic interferogram was derived from 15 interferograms spanning six SAR acquisition dates.

InSAR Processing of Isolated Coherent Scatterers

In assessing InSAR time series techniques, we decided that developing a coherent scatterer InSAR processing capability is important to the success of the project. For the general application of InSAR, the variation of the atmosphere over time and space results in artifacts masking deformation features. In addition, the presence of vegetation results in widespread decorrelation over time for C-band InSAR. The purpose of coherent scatterer InSAR analysis is to use several interferograms spanning different time spans to separate atmospheric delays from surface deformation [Ferretti et al., 2001; Ferretti et al., 2000]. We utilize Phoenix data already in hand to create full-resolution InSAR results for use in coherent scatterer algorithm development and application.

Coherent scatterer InSAR processing is performed on an irregular grid of interferogram pixels that remain coherent over long periods of time. A sequence of differential interferograms is created, each relative to the same reference date. In general, these interferograms cannot be unwrapped due to temporal decorrelation and large interferometric baselines. However, there remains a subset of sparse useable phase data associated with coherent subpixel scatterers.

An initial set of coherent scatterers is identified from pixels with low radar backscatter dispersion over the stack of SAR images (Figure 5). For each initial coherent scatterer pixel, phase differences are formed with neighboring coherent scatterers. Relative (differences in) displacement velocities and height errors are estimated between pairs of coherent scatterers by maximizing the single-pixel multi-interferogram correlation. With the gradients estimated, the relative velocities, height errors and phases can be unwrapped (Figure 6). Various high and low pass filters are applied in time and space to separate atmospheric artifacts from nonlinear deformation. The process is then repeated to find additional coherent scatterers.

The benefit of coherent scatterer analysis is that it might have success in regions where conventional InSAR fails due to temporal decorrelation. The success of coherent scatterer InSAR depends, in part, on the density of coherent scatterers in the area of interest. Because of the determination and removal of the atmospheric phase contribution, coherent scatterer InSAR has the potential to detect millimeter per year deformation rates.

New SAR Modes of Operation

As the successor to ERS, Envisat was launched in March 2002 with SAR data acquisitions available from September 2002. Envisat SAR characteristics include the following:

- spatial and radiometric resolution, sensitivity and ambiguity suppression similar to ERS
- improved orbits due to DORIS microwave tracking instrument (more accurate orbits will result in more accurate and automated InSAR data processing relative to ERS)
- multiple polarizations, including an Alternating Polarization Mode, as compared with fixed polarization for ERS (using an alternative polarization may provide improved InSAR coherence in certain locations due to different scattering mechanisms)
- seven swaths ranging in incidence angles from 15 to 45 degrees

InSAR data from multiple satellite passes can be combined to constrain, reveal the spatial extent, and determine more than the line-of-sight displacement associated with a deformation event captured in a set of interferograms. For example, Fialko et al. [2001] reveal the three-dimensional coseismic displacement field of the October 1999 Hector Mine earthquake through the use of InSAR from descending and ascending satellite passes as well as from the azimuth offsets determined as part of the registration of the SAR images used to form the descending pass interferogram. Peltzer et al. [1999] utilized the InSAR offsets and data from three adjacent satellite tracks to capture the 170-km-long surface rupture associated with the November 1997 Manyi, Tibet earthquake.

Acquisitions from multiple SAR swaths can also provide valuable additional data for identifying subtle deformation features or deformation rates that vary over time. The overlap of adjacent SAR swaths affords the opportunity to image a deformation feature at additional times. The amount of overlap is determined by the SAR operating mode, latitude of study site and how the SAR processing is implemented. For example, for the fixed viewing geometry of ERS, adjacent SAR swaths over Phoenix overlap by approximately one-third when processed to the full extent possible in slant range. More overlap occurs as satellite tracks converge at the poles. In contrast, Envisat provides flexible swath positioning at different incidence angles. This is a powerful new capability relative to ERS, which assures that a deformation feature of interest can be imaged by two adjacent tracks as well as on both descending and ascending satellite passes.

A sample of Envisat SAR data over Hokkaido, Japan was used for developing and testing Envisat SAR and InSAR processing capability (Figure 7). We intend to use Envisat swath positioning to image deformation features of interest from multiple satellite tracks. This will greatly increase the amount of InSAR data available for use with advanced InSAR processing techniques. A detailed comparison will be made between previous ERS InSAR results and new Envisat results to quantify the anticipated improvements to seismic event location and source mechanism determination capabilities.

HISTORICAL PERSPECTIVE

It was recently demonstrated that InSAR can play a significant role in providing accurate GT for both seismic event location calibration and discrimination purposes, and is especially valuable in denied or difficult-access regions. For example, InSAR has been applied to nuclear explosion monitoring efforts at LLNL by creating deformation maps of the NTS and other nuclear test sites, as well as mine collapses and moderate earthquakes in the Middle East [Vincent, et al., 1999; Vincent, et al., 2000; Swenson, et al., 2001; Vincent, et al., 2001; Walter, et al., 2001; Myers, et al., 2002; Vincent et al, 2002; Walter, et al., 2002]. A review of InSAR and its technical challenges follows.

Differential Interferometry

SAR is an active microwave coherent (phase preserving) imaging remote sensing instrument. Typical satellite SAR can collect data along ~100 km imaging swaths on both ascending and descending satellite passes. In differential InSAR studies, the difference in the phases of nearly-coincident SAR images collected at different times are related to surface topography as well as any deformation that may have occurred along the radar line-of-sight. The deformation signature is isolated by removing the phase due to topography using either another interferogram that contains only topographic phase information, or by using an independent digital elevation model to simulate the topographic phase.

Differential InSAR has developed into a viable and valuable tool for measurement of earth-surface deformation associated with natural and anthropogenic hazards such as seismic activity [Peltzer et al., 2001a; Sandwell et al., 2000; Bürgmann et al., 1998; Zebker et al., 1994] and subsidence associated with subsurface fluid withdrawal [Bawden et al., 2001; Hoffmann et al., 2001; Galloway et al., 1998; Fielding et al., 1998]. InSAR scientific studies have progressed from single interferogram investigations of line-of-sight deformation over a given time period [Massonnet et al., 1993] to multi-interferogram reconstructions of three-dimensional displacements [Fialko et al., 2001] and InSAR time series of continuous but variable deformation [Berardino et al., 2001].

InSAR Technical Challenges

The primary limitations of repeat-pass InSAR are temporal and geometric decorrelation, artifacts in the interferogram as the result of atmospheric variations between acquisitions, and to a lesser degree, imprecise knowledge of the interferometric baseline [Table 1, Sandwell and Sichoix, 2000]. Temporal decorrelation occurs when individual scatterers within a pixel are rearranged or move incoherently by a distance on the order of the radar wavelength or greater between acquisitions. At the ERS C-band 6-cm wavelength, urban areas are generally well-correlated but widespread decorrelation is observed in vegetated areas. At longer wavelengths, e.g., L-band, vegetation penetration is possible and results in more coherence in lightly vegetation areas, although cultivated agricultural fields still decorrelate over time. Geometric decorrelation is a result of the direct relationship between the interferometric baseline and the maximum correlation between the SAR images, i.e., at the critical baseline, the maximum correlation decreases to zero. For ERS, the critical baseline is ~1100m, with a practical baseline limit of ~400m for conventional InSAR applications.

Atmospheric artifacts are associated with variations in the ionosphere and troposphere, with spatial and temporal variations in water vapor typically being the largest source of error. These variations occur on many spatial scales, from kilometer-scale artifacts that appear similar to localized subsidence features, to large-scale phase ramps spanning much of the interferogram. Imprecise knowledge of the baseline results in similar broad-scale residual phase ramps across the flattened interferogram. However, these phase ramps can be removed with a few topographic or deformation control points distributed across the image.

Differential interferograms contain the deformation signature of interest as well as several other contributions, such as residual topography and atmospheric artifacts. For differential interferogram phase signatures greater than a cycle and spatial extent less than the size of the interferogram, visual inspection of a few interferograms can be used to confirm that the signature is surface deformation. In other words, phase signatures that are persistent across several independent interferograms are likely related to deformation. For analyses of many interferograms and more subtle and complex deformation (e.g., mm- to cm-scale interseismic displacement or time-varying subsidence), these ad-hoc qualitative comparisons are neither satisfying nor tractable.

CONCLUSIONS

InSAR time series approaches have several advantages when compared with the ad-hoc consideration of individual interferograms. Shorter period interferograms in the time series analysis results in useful cumulative deformation measurements at pixels that otherwise decorrelate in a single or few longer period interferograms spanning the total period of the time series. We are working on various interferogram weighting schemes to take into consideration phase noise associated with decorrelation and height error propagation for each interferogram to better address the contribution of noisy interferograms in the solution process. The use of the coherent scatterer InSAR processing provides a means to isolate differential interferometric phase signatures (deformation, atmospheric artifacts, topographic phase residuals due to digital elevation model height errors) on a subset of pixels in an otherwise noisy set of interferograms. This allows for the detection of millimeter-level deformation signals over time.

ACKNOWLEDGEMENTS

ERS original SAR data provided by the European Space Agency copyright 1993-2000. Additional data purchases made by the WInSAR consortium with funding from NASA, USGS, and NSF.

REFERENCES

Bawden, G., W. Thatcher, R. Stein, K. Hudnut, G. Peltzer, Tectonic contraction across Los Angeles after removal of groundwater pumping effects, Nature, 412, Aug. 23, 2001.

Berardino, P., G. Fornaro, A. Fusco, D. Galluzzo, R. Lanari, E. Sansosti, S. Usai, A new approach for analyzing the temporal evolution of Earth surface deformations based on the combination of DIFSAR interferograms, Int. Geosci. Rem. Sens. Symp., Sydney, Australia, July 9-13, 2001.

Buckley, S., Radar Interferometry Measurement of Land Subsidence, Ph.D. dissertation, The University of Texas at Austin, 2000.

Bürgmann, R., E. Fielding, J. Sukhatme, J., Slip along the Hayward fault, California, estimated from space-based synthetic aperture radar interferometry, Geology, 26(6), 559-562, 1998.

Ferretti, A., C. Prati, F. Rocca, Permanent Scatterers in SAR Interferometry, IEEE Trans. Geosci. Rem. Sens., 39(1), 2001.

Ferretti, A., C. Prati, F. Rocca, Nonlinear Subsidence Rate Estimation Using Permanent Scatterers in Differential SAR Interferometry, IEEE Trans. Geosci. Rem. Sens., 38(5), 2000.

Fialko Y., M. Simons, D. Agnew, The complete (3-D) surface displacement field in the epicentral area of the 1999, Mw 7.1, Hector Mine earthquake from space geodetic observations, Geophys. Res. Lett., 28(16), 3063–3066, 2001.

Fielding, E., R. Blom, R. Goldstein, Rapid Subsidence over Oil Fields Measured by SAR Interferometry, Geophys. Res. Lett., 25(17), 3215-3218, 1998.

Galloway, D., K. Hudnut, S. Ingebritsen, S. Philips, G. Peltzer, F. Rogez, P. Rosen, Detection of aquifer system compaction and land subsidence using interferometric synthetic aperture radar, Antelope Valley, Mojave Desert, CA, Water Resour. Res., 34(10), 2573–2586, 1998.

Goldstein, R., C. Werner, Radar Interferogram Filtering for Geophysical Applications, Geophys. Res. Lett., 25(21), 4035, 1998.

Gudipati, K., S. M. Buckley and C. R. Wilson, Temporal Variations in Phoenix, Arizona Subsidence from Radar Interferometry, submitted to Geophys. Res. Lett., 2004.

Hoffmann, J., H. Zebker, D. Galloway, F. Amelung, Seasonal subsidence and rebound in Las Vegas Valley, Nevada, observed by synthetic aperture radar interferometry, Water Resour. Res., 37(6), 1551-1566, 2001.

Lundgren, P., S. Usai, E. Sansosti, R. Lanari, M. Tesauro, G. Fornaro, P. Berardino, Modeling Surface Deformation observed with SAR Interferometry at Campi Flegrei Caldera, J. Geophys. Res., 106(B9), 19355-19367, 2001.

Massonnet, D., M. Rossi, C. Carmona, F. Adragna, G. Peltzer, K. Feigl, T. Rabaute, The Displacement Field of the Landers Earthquake Mapped by Radar Interferometry, Nature, 364, 138-142, July 8, 1993.

Myers, S.C., M. Flanagan, M. Pasyanos, W. Walter, P. Vincent, and C. Schultz, Location calibration in Western Eurasia and North Africa: ground truth, improved earth models, Bayesian kriging, regional analysis, location algorithms, array calibration, and validation, Proceedings of the 23rd Seismic Research Review, 2002.

Peltzer, G., F. Crampé, P. Rosen, The Mw 7.1, Hector Mine, California earthquake: surface rupture, surface displacement field, and fault slip solution from ERS SAR data, Earth and Plaentary Sciences, 333, 545-555, 2001a.

Peltzer, G., F. Crampé, S. Hensley, P. Rosen, Transient strain accumulation and fault interaction in the Eastern California shear zone, Geology, 29(11), 975–978, 2001b.

Peltzer, G., F. Crampé, G. King, Evidence of Nonlinear Elasticity of the Crust from the Mw7.6 Manyi (Tibet) Earthquake, Science, 286, 272-276, Oct. 8, 1999.

Sandwell, D., L. Sichoix, D. Agnew, Y. Bock, J.-B. Minster, Near real-time radar interferometry of the Mw 7.1 Hector Mine Earthquake, Geophys. Res. Lett., 27(19), 3101-3105, 2000.

Sandwell, D. and L. Sichoix, Topographic phase recovery from stacked ERS interferometry and a low-resolution digital elevation model, J. Geophys. Res., 105(B12), 28211-28222, 2000.

Sandwell, D. and E. Price, Phase gradient approach to stacking interferograms, J. Geophys. Res., 103(B12), 30183-30204, 1998.

Schmidt, D. A. and R. Bürgmann, Time-dependent land uplift and subsidence in the Santa Clara valley, California, from a large interferometric synthetic aperture radar data set*, J. Geophys. Res., 108(B9)*, 2416, doi:10:1029/2002JB002267, 2003

Swenson, J.L., W. Foxall, W.R. Walter and P. Vincent (2000). Source characterization of the February 3, 1995 and January 30, 2000 mine collapses in the trona mining district of southwestern Wyoming from InSAR and seismic waveform modeling, EOS, Transactions 81, S8.

Usai, S., A New Approach for Long Term Monitoring of Deformations by Differential SAR Interferometry, Ph.D. Dissertation, Delft University of Technology, The Netherlands, 2001.

Vincent, P., Final Report (00-ERD-056) MEDIOS: Modeling Earth Deformation Using Interferometric Observations from Space, LLNL, UCRL-ID-146985, 2002.

Vincent, P., J. Sweeney, Utility of InSAR for Test Site Monitoring, LLNL, UCRL-ID-150194 (OUO), 2003.

Vincent, P., S. Larsen, D. Gallaway, R.J. Laczniak, W. R. Walter, B. Foxall, J. Zucca, New signatures of underground nuclear tests revealed by satellite radar interferometry, LLNL, UCRL-JC-145562, 2001.

Vincent, P., Using satellite radar interferometry to detect and characterize HDBTs, NPAC TWG R and D Conference on Detecting, Characterizing and Defeating Underground Facilities, April 3-4, 2001 (INVITED).

Vincent, P., B. Foxall, W. R. Walter, Analysis, comparison and modeling of radar interferometry data of surface deformation signals associated with underground explosions, mine collapses and earthquakes, PHASE 1: Underground explosions, Nevada Test Site, 21st Seismic Research Symposium on Monitoring a Comprehensive Test Ban Treaty, Las Vegas, NV, September 21-23, 1999.

Walter, W. R., J. Swenson, W. Foxall, P. Vincent, A. J. Rogers, J. Bhattacharyya, Complete regional waveform modeling for source and structure: A source example using the January 30, 2000 mine collapse in Wyoming, 12th Annual IRIS Workshop, Rockport, Maine, May 7-10, 2000.

Walter, W. R., P. Vincent, S. C. Meyers, Joint Seismic Waveform and InSAR Modeling of Moderate Earthquakes in Iran, EOS Transactions, AGU Fall, 2002.

Zebker, H., P. Rosen, R. Goldstein, A. Gabriel, C. Werner, On the Derivation of Coseismic Displacement Fields Using Differential Radar Interferometry: The Landers Earthquake, J. Geophys. Res., 99(B10), 19617-19634, 1994.

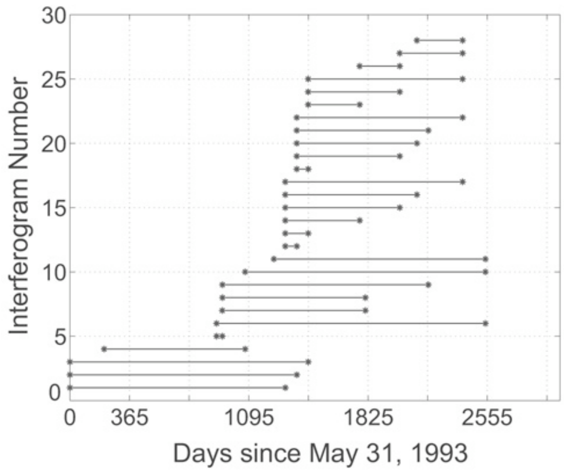

Figure 1. Distribution of Phoenix interferograms used in linear inversion [from Gudipati, Buckley and Wilson, 2004].

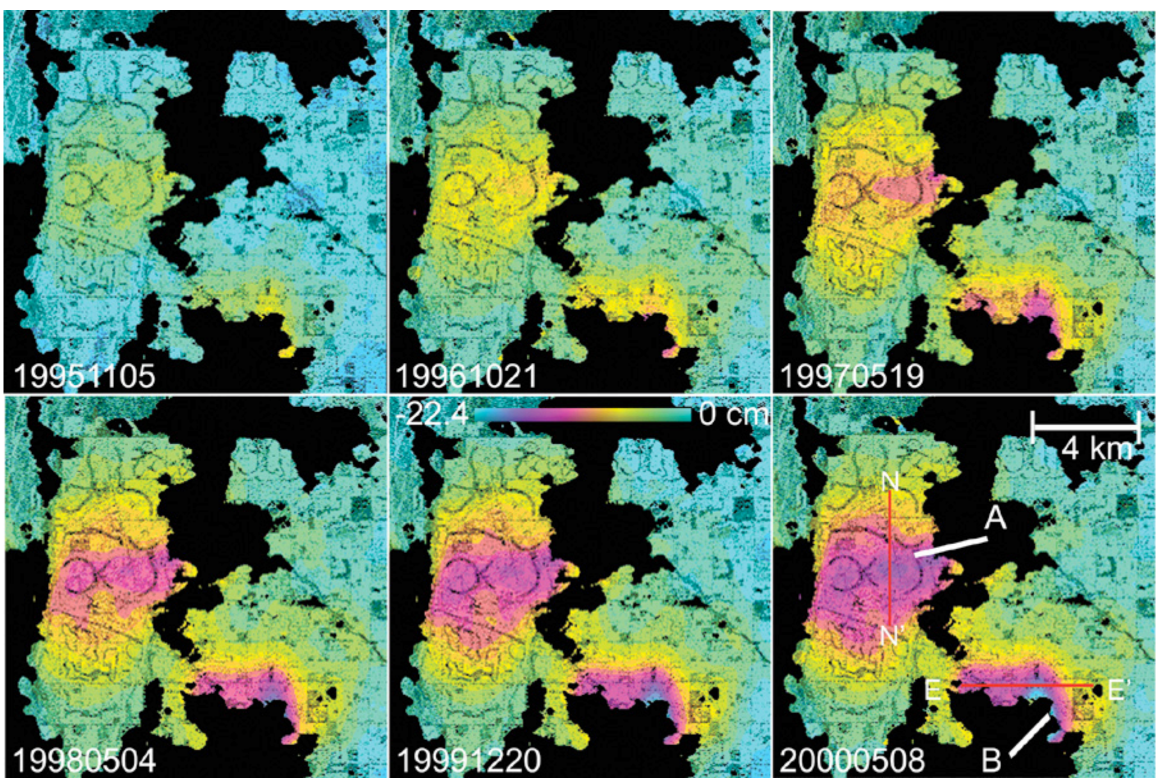

Figure 2. Cumulative subsidence since May 21, 1993 in Glendale near Phoenix. Black corresponds to areas of decorrelation. [from Gudipati, Buckley and Wilson, 2004].

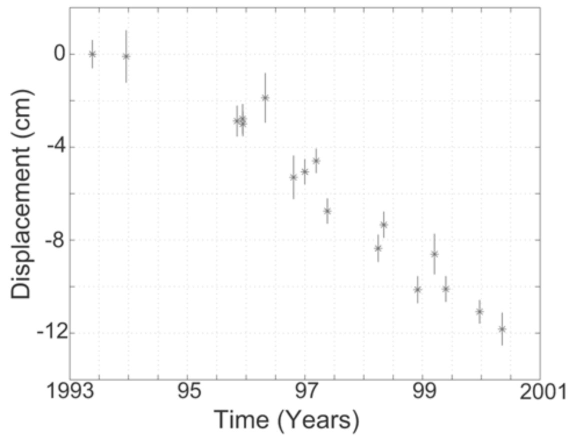

Figure 3. Mean subsidence near the maximum observed subsidence of feature B. Mean computed along profile EE' in Figure 2. Error bars correspond to one standard deviation phase error mapped from correlation and digital elevation model height error [from Gudipati, Buckley and Wilson, 2004].

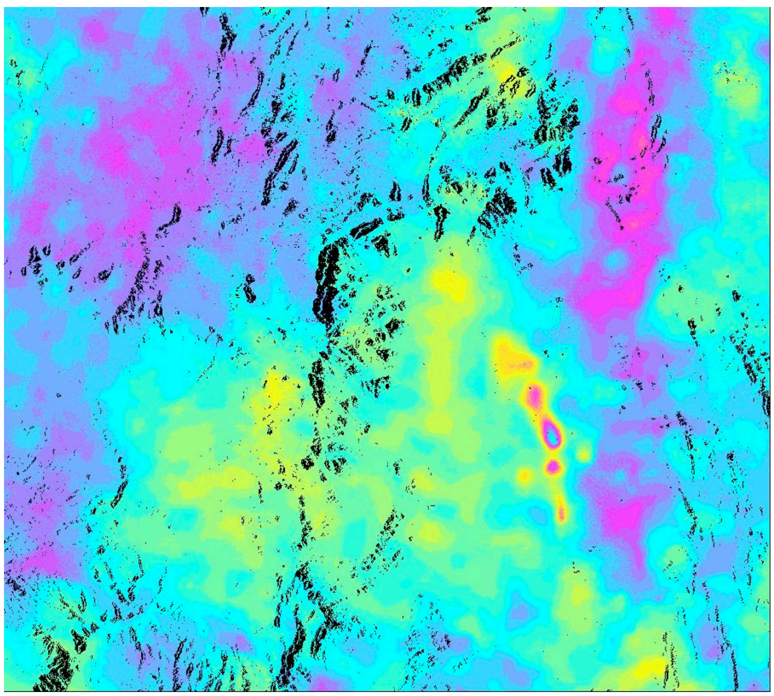

Figure 4. Preliminary time series result showing cumulative displacement over the Nevada Test Site from June 11, 1995 to June 16, 1997. One cycle through color wheel represents 5 cm of radar line-of-sight displacement.

Figure 5. Initial coherent scatterers identified in Scottsdale near Phoenix.

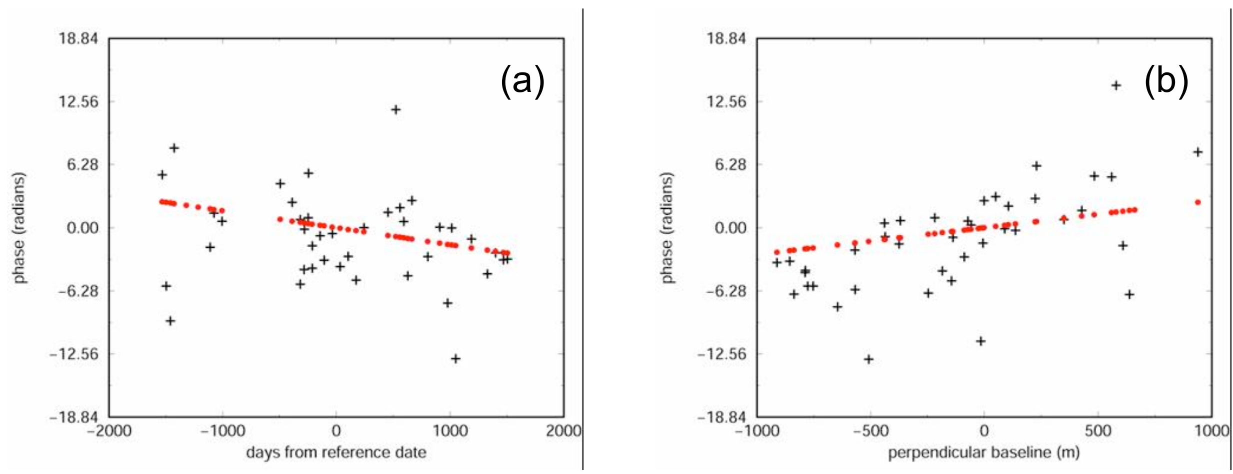

Figure 6. Sparse unwrapping result for a single coherent scatterer observed in a preliminary set of Scottsdale interferograms. Coherent scatterer velocity and height error estimated as 3 mm/yr and 3 meters, respectively. (a) Coherent target interferogram phases after removal of height error phase contribution. Red is estimated velocity phase contribution. (b) Coherent scatterer interferogram phases after removal of estimated velocity phase contribution. Red is estimated height error phase contribution. Large phase dispersion likely due to residual phase ramps in preliminary interferograms. Refinement of interferograms will lead to improved estimates and smaller phase dispersion.

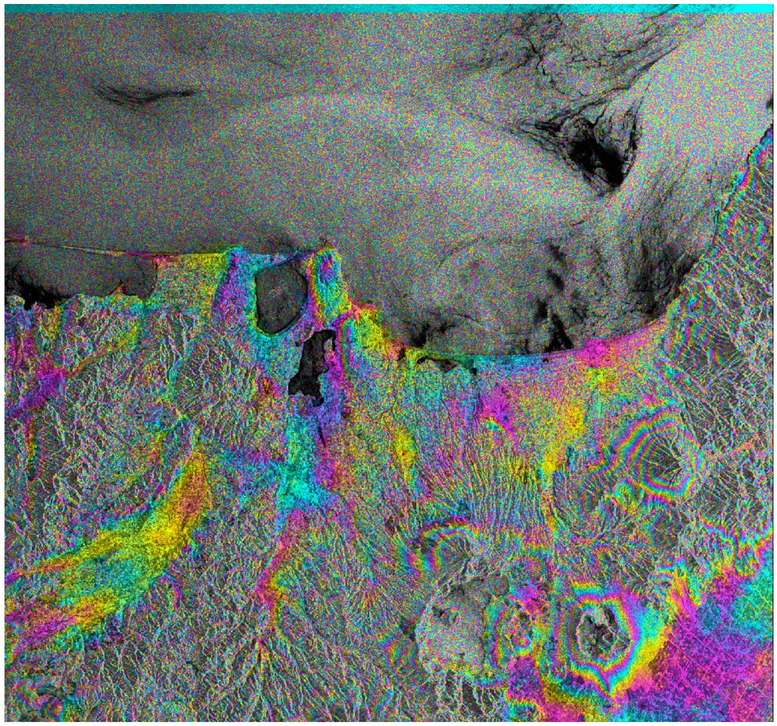

Figure 7. Hokkaido, Japan Envisat flattened interferogram spanning August 24 to September 28, 2003.